

Temperature Field and Stress Field Distribution of Forged Steel Brake Disc for High Speed Train

Ruoqi Suo^{*}, Xiaoling Shi

Department of Mining Engineering, Luliang University, Luliang 033000, China

Received 14 July 2021

Accepted 22 December 2021

Abstract

Thermal load plays a great role in brake disc failure, which seriously threatens the safety of train running. In this paper, the thermal elastic-plastic constitutive relation of the brake disc is obtained by experimental test, and the stress-strain response relationship of brake disc under different braking conditions is simulated by using the numerical calculation based on sequential coupling method. The temperature field and stress field are calculated under once 200 km/h emergency braking, once 300 km/h emergency braking, once 29 kN constant pressure braking and three times of 29 kN successive constant pressure braking. The results show that the worse the braking condition, the greater the temperature field and stress field. The temperature field decreases along the thickness direction; increases first and then decreases along the radial direction. During the braking process, the circumferential stress is the principal stress on the disc surface and the different residual tensile stress is formed after four braking conditions. The speed value has the greatest influence on the temperature field and stress field. These findings provide a reference for the thermal fatigue life evaluation of the high-speed train brake disc.

© 2022 Jordan Journal of Mechanical and Industrial Engineering. All rights reserved

Keywords: Brake disc; Temperature field; Thermal stress; Residual stress; Thermal elastic-plastic;

1. Introduction

The thermal fatigue crack on the surface of the brake disc is closely related to the stress state in service, the structure and material [1-6]. The domestic and international researchers have conducted in-depth research on temperature field and stress field [7-13]. Yevtushenko and Greza, Anderson and Knapp found that thermal stress caused by high temperature can lead to disc surface crack or permanent deformation of brake disc [14, 15]. The friction, thermal deformation and elastic contact between brake disc and brake pad will also influence the change of contact pressure and surface temperature. Belhocine and Bouchetara simulated the coupling behavior between temperature field and stress field of automobile brake disc by thermal structure sequential coupling method [16]. It was found that stress concentration was easy to arise at the joint of brake disc and wheel, and cracks may occur after multiple braking. Ghadimi et al. found that the heat generated during friction between brake disc and brake pad has a lot of adverse effects on the brake system, such as braking performance, premature wear, thermal crack and brake disc thickness change [17]. Choj and Lee, Su et al., Gao et al. used the finite element method to analyze the thermo elastic contact between the brake disc and the brake pad [18-20]. Based on the theory of coupled heat conduction and elastic equation, the thermal stress under successive braking is calculated, and the influence of thermoelastic instability (TEI) on thermoelastic behavior is studied. Kim et al. established a three-dimensional ventilation brake disc model, and analyzed the distribution

law of thermal stress of brake disc under two different conditions of uniform contact pressure and non-uniform contact pressure [21]. Adamowicz and Grzes, Li et al., Zhu et al., Chai et al. established two-dimensional and three-dimensional brake disc models [22-25]. By comparing the temperature field distribution of the two models under the action of non axisymmetric load, it is found that the temperature field calculation results based on the three-dimensional brake disc model are lower than those of the two-dimensional brake disc model, thus affecting the thermal stress field distribution of the brake disc. These results provide a theoretical basis for the development and design of brake disc [26-30]. In this paper, the elastic-plastic finite element method is used to analyze the temperature field and stress field distribution of brake disc under different braking conditions, so as to achieve a better heat and stress distribution on the surface [31].

2. Theoretical Analysis

When the expansion or contraction caused by the temperature change of the object is constrained, thermal stress will be generated inside the structure, and the thermal stress is $\alpha \times (T_r - T_0)$. Where α is the thermal expansion coefficient of the material, which changes with the change of temperature and material. T_r is the temperature corresponding to the time τ , which T_0 is room temperature [32-35].

* Corresponding author e-mail: llxysrq@163.com.

When the stress function of material yield is set to f , the yield function is satisfied by $f = 0$. Then the forged steel material meets Mises yield condition:

$$f = J_2 - K^2 = 0 \tag{1}$$

where, K is the yield stress under shear condition; J_2 is the second invariant of stress deviator.

Based on the theory of thermodynamics, thermal stress is mainly caused by temperature gradient. It is assumed that $t = t(r)$, for isotropic materials, the strain components in polar coordinates in the elastic range are:

$$\begin{aligned} \varepsilon_r &= \frac{1}{E}[\sigma_r - \mu(\sigma_\theta + \sigma_z)] + \alpha t \\ \varepsilon_\theta &= \frac{1}{E}[\sigma_\theta - \mu(\sigma_r + \sigma_z)] + \alpha t \\ \varepsilon_z &= \frac{1}{E}[\sigma_z - \mu(\sigma_\theta + \sigma_r)] + \alpha t \\ \gamma_{rz} &= \frac{1}{G}\tau_{rz} = \frac{2(1+\mu)}{E}\tau_{rz} \end{aligned} \tag{2}$$

$$\varepsilon_{r0} = \varepsilon_{\theta 0} = \varepsilon_{z0} = \alpha t, \gamma_{rz0} = 0$$

The second invariant of stress deviation J_2 is:

$$\begin{aligned} J_2 &= \frac{1}{6}[(\sigma_r - \sigma_\theta)^2 + (\sigma_\theta - \sigma_z)^2 + (\sigma_z - \sigma_r)^2 \\ &\quad + (\sigma_r - \sigma_\theta)^2 + 6(\tau_{rz}^2 + \tau_{rz}^2 + \tau_{rz}^2)]^{1/2} \\ &= \frac{1}{6}[(\sigma_1 - \sigma_2)^2 + (\sigma_2 - \sigma_3)^2 + (\sigma_3 - \sigma_1)^2]^{1/2} \end{aligned} \tag{3}$$

According to Formula (1), the plastic yield condition of forged steel material uses Mises criterion [36]. Considering the influence of strain during plastic deformation, the yield function can be expressed as:

$$f = f(\sigma_r, \sigma_\theta, \sigma_z, \tau_{rz}, \tau_{rz}, \tau_{rz}, \varepsilon_r^p, \varepsilon_\theta^p, \varepsilon_z^p, \lambda_{rz}^p, \lambda_{rz}^p, \lambda_{rz}^p) = 0 \tag{4}$$

If the influence of temperature T is considered, the corrected yield function is:

$$f = f(\sigma_r, \sigma_\theta, \dots, \varepsilon_r^p, \varepsilon_\theta^p, \dots, T) = 0 \tag{5}$$

During the running of the brake disc, the mechanical stresses such as the brake pad pressure and friction force

between the brake pad and the brake disc interact with the thermal stress during the braking process [37-40]. Hence, when mechanical stress and thermal stress work together, the relationship between stress and strain is:

$$[K]\{\delta\} = \{R\}_T + \{R\} \tag{6}$$

where $[K]$ represents the total stiffness matrix; $\{R\}$ represents the mechanical stress; $\{R\}_T$ represents the thermal stress; $\{\delta\}$ represents the node displacement.

It can be seen that the total structural deformation caused by mechanical stress and thermal stress can be obtained according to the superposition principle.

3. Modeling for Calculation

3.1. Finite element model

The braking process of high-speed train is the process of converting kinetic energy into heat energy. Relevant studies have shown that only about 20% of the heat generated by friction between the brake disc and the brake pad is consumed on the contact surface, and about 80% of the energy is transferred to the sub-surface material of the brake disc [41-44]. Therefore, the temperature field of the brake disc is not only unstable, but also the volume heat generated by the interface layer. The finite element grid and related parameters of the brake disc are shown in Figure 1 and Table 1.

Table 1. Related dimensions of brake disc and pad

Category	Outer diameter/mm	Inside diameter/mm	Thickness/mm	Coverage angle/°
Brake disc	36.0	22.3	53.3	64.5
pad	35.5	23.7	20.0	100

When dividing the three-dimensional finite element mesh, the friction surface part of the brake disc adopts a hexahedral mesh, the heat dissipation rib uses a tetrahedral mesh, and the brake pad adopts a hexahedral mesh. The divided finite element mesh has a total of 66948 elements. There are 15516 hexahedral meshes and 51432 tetrahedral meshes.

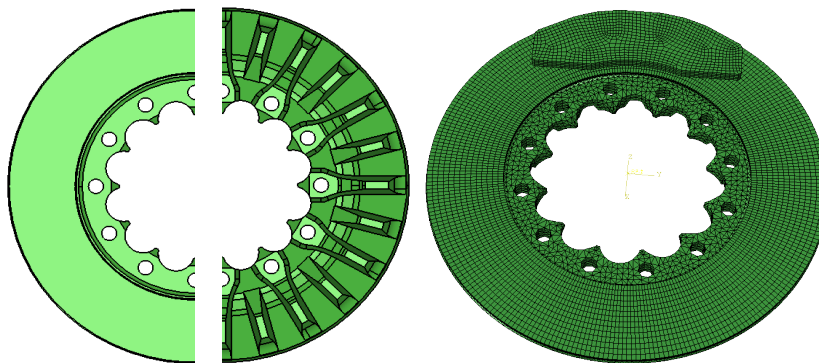


Figure 1. The geometric model and finite element model of brake disc and pad

3.2. Material parameters

The material is subjected to monotonic tensile tests at room temperature and high temperature, and the strain amplitude control method is adopted in the test and test temperatures are as follows: 25 °C, 100 °C, 200 °C, 300 °C, 400 °C and 500 °C. The stress-strain curve of monotonic tension is shown in Figure 2, which the test values are the average of three valid tests.

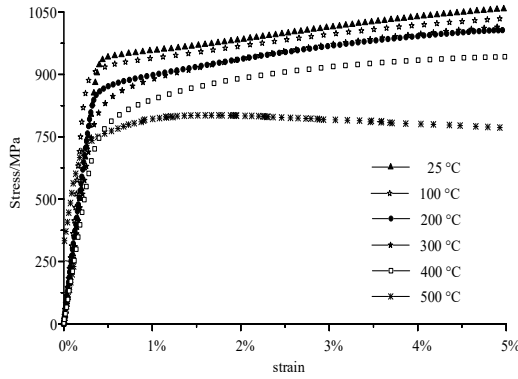


Figure 2. Monotonic tensile curve of $\sigma - \varepsilon$

Table 2 shows the material parameters at different temperatures. Considering that Poisson's ratio and density are not affected by temperature, they are regarded as constants. The yield strength, elastic modulus and thermal conductivity of the material decrease obviously with temperature, while the specific heat capacity and thermal expansion coefficient increase with temperature.

3.3. The boundary conditions

According to the technical requirements and actual operation curve of high-speed train foundation braking [45-48], four typical working conditions are calculated, including once emergency braking at 200 km/h, once emergency braking at 300 km/h, once 29 kN constant pressure braking at 200 km/h and three times of 29 kN successive constant pressing braking at 200 km/h. The bolt hole is fully constrained in the calculation process. Figure 3 illustrates the variation curves of brake pad pressure and braking speed with braking time under the speed levels of 200 km/h and 300 km/h. Figure 4 shows the variation curves of brake pad pressure and braking speed with braking time under one 29 kN constant pressure braking and three times of 29 kN successive constant pressure braking.

Table 2. Mechanical properties and thermophysical parameters at different temperatures

Temperature (°C)	Elastic modulus/E (GPa)	Yield strength (MPa)	Specific heat capacity (Cp/J/gK)	linear expansion coefficient (10 ⁻⁶ /°C)	Thermal conductivity /(W/m·°C)
25°C	228	790	0.485	10.9	45.2
100°C	224	710	0.485	10.9	45.0
200°C	223	670	0.515	11.7	42.7
300°C	207	590	0.550	12.3	40.5
400°C	177	450	0.555	12.8	37.6

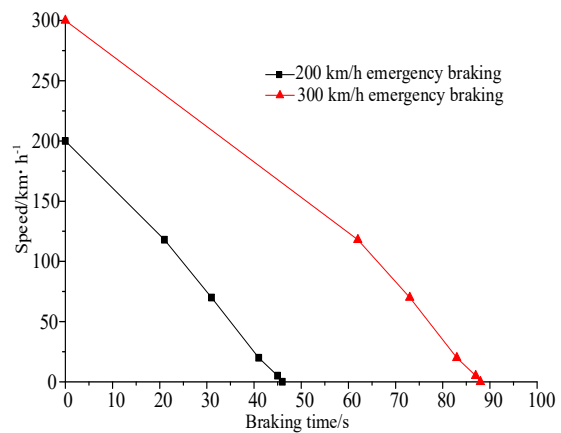
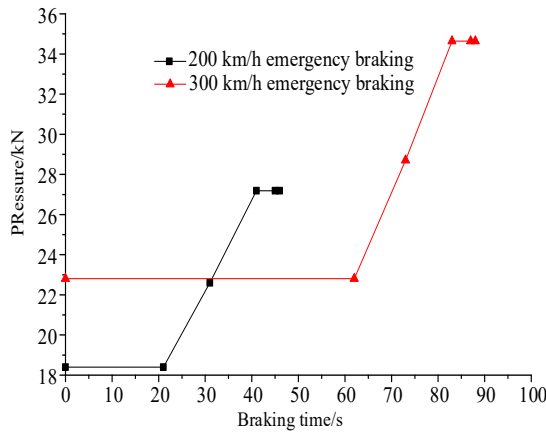


Figure 3. The emergency braking force curve

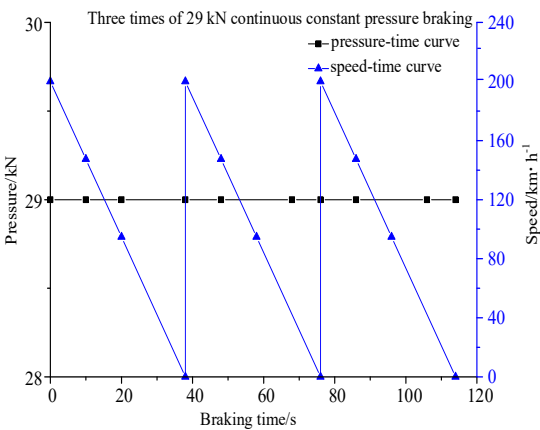
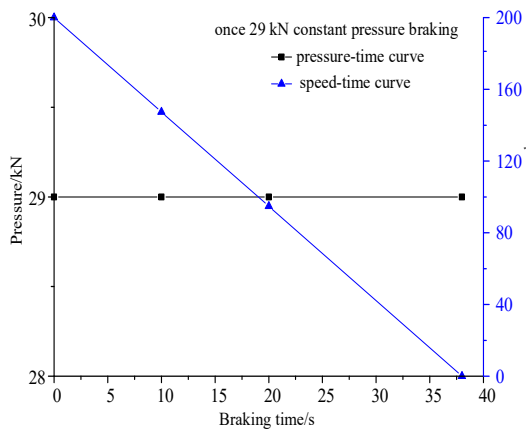


Figure 4. The constant pressure brake curve

As shown in Figure 3, the heat input is the highest under 300 km/h emergency braking. The maximum pressure under 200 km/h emergency braking and 300 km/h emergency braking is 27.18 kN and 34.64 kN respectively. It can be seen from Figure 4 that under the speed level of 200 km/h, there is a linear relationship between the speed curve of 29 kN constant pressure braking and the braking time. After braking, the natural convection and heat dissipation occur between brake disc and air. After 30 minutes later, the surface temperature of 200 km/h emergency braking will return to room temperature.

3.4. Other calculation parameters

In this study, the ambient temperature is $T(X, Y, Z) = 25\text{ }^\circ\text{C}$ at time $t = 0\text{ s}$. The input heat flow is obtained by using the friction power method. The effective friction area of the brake disc is 0.21 m^2 , the friction coefficient is 0.28, and the effective radius of the brake disc is 297.3 mm. During the braking process, the brake disc is in forced convection heat dissipation state, and the heat dissipation coefficient is taken as $120\text{ W/m}^2\cdot^\circ\text{C}$ at 200 km/h; After braking, the brake disc is in natural convection heat dissipation state, with the value of $28\text{ W/m}^2\cdot^\circ\text{C}$, and the linear value is taken during braking. In the braking process, the indirect coupling method is used for calculation. The bilinear isotropic strengthening criterion

is adopted in the thermal stress calculation, and the structural analysis element solid 185 is used to replace the thermal analysis element solid 70 for nonlinear transient analysis.

4. Calculation Results

4.1. Temperature field results

In order to study the stress distribution of the brake disc, that is, the distribution law of the thermal stress of the brake disc with the thickness and radial direction, the temperature field distribution of the brake disc is first analyzed. Select five positions along the radial direction. The distances from the center of the brake disc are 223 mm, 243 mm, 263 mm, 283 mm, and 303 mm. The node numbers are 41487, 41431, 41430, 41353, 41379. Four positions are selected along the thickness direction, and their distances from the friction surface are 0 mm, 6 mm, 16 mm, 38 mm. The node numbers are 41430, 41960, 42233, 42242, as shown in Figure 5. Under different braking conditions, the temperature change curve along the thickness direction is shown in Figure 6, and the temperature change curve along the radial direction is shown in Figure 7.

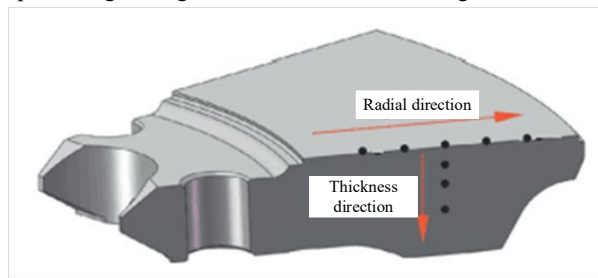


Figure 5. The temperature and stress measuring point of brake disc

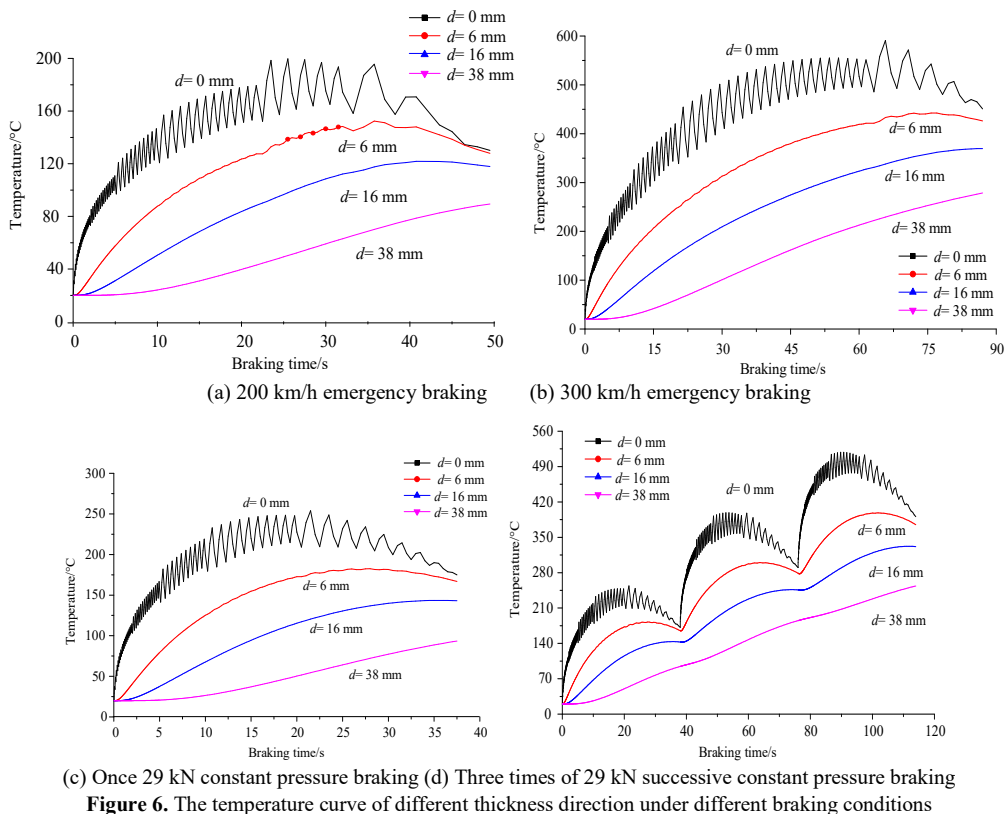


Figure 6. The temperature curve of different thickness direction under different braking conditions

It is found that at the beginning of braking, with the successive input of strong heat flow, the surface heats up rapidly in a short time and reaches the peak point soon in Figure 6. Then, due to the effect of forced convection cooling, the surface gradually transfers heat to the disk body through heat conduction, thus the temperature gradually drops. At the same time, the temperature field of the brake disc gradually decreases along the thickness direction. This is because the strong friction between the brake disc and the brake pad that causes the surface temperature to rise sharply in a short time, while the temperature inside the brake disc is caused by heat

conduction. Therefore, the greater the distance d from the friction surface, the lower the temperature.

Figure 7 shows that the temperature field of the disc surface increases first and then decreases in the radial direction. This is due to: (1) Limited by the geometric structure of the brake disc; (2) The friction ring is located at the center of the disc surface, closer to the center of the disc surface, the slower the heat dissipation, the higher the temperature. The cloud diagram of brake disc transient temperature field under different working conditions is shown in Figure 8.

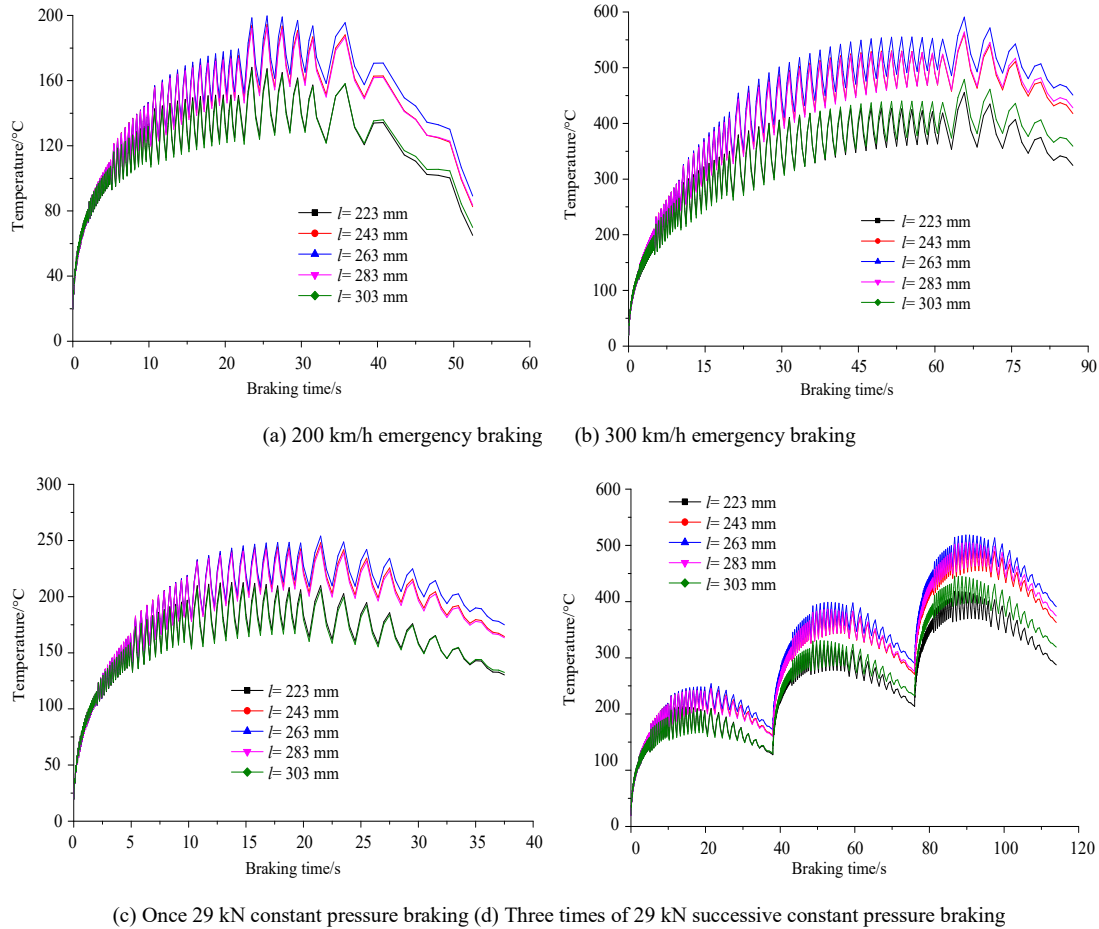


Figure 7. The temperature curve of different radial direction under different braking conditions

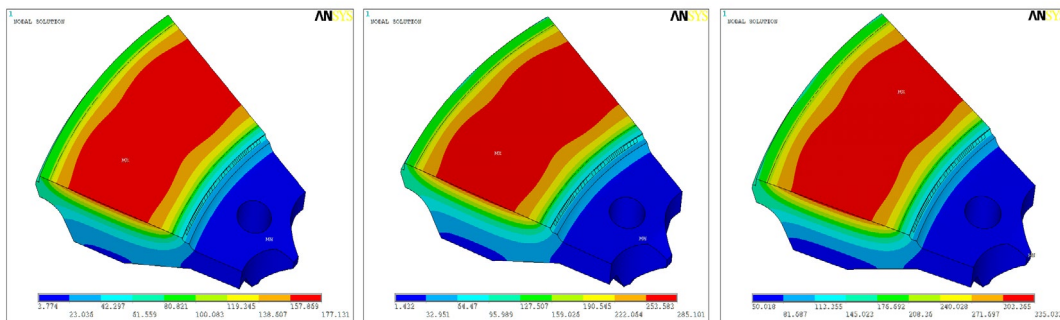


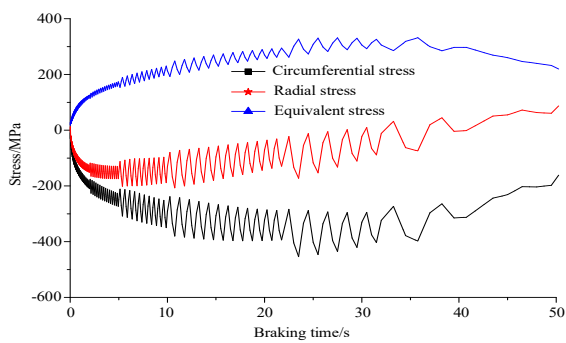
Figure 8. The cloud diagram of temperature field under different braking conditions

It can be seen from Figures 6-8 that the temperature field changes under different braking conditions are relatively similar. At the beginning of braking, the heat flux density is the largest, and during the braking process, the heat flux density gradually decreases as the braking time increases. The temperature field of the brake disc also shows a similar law under different braking conditions, that is, the temperature growth rate is getting smaller and smaller. After reaching the peak, the temperature of the disk gradually decreases. After braking, the temperature of the disc body gradually returns to room temperature.

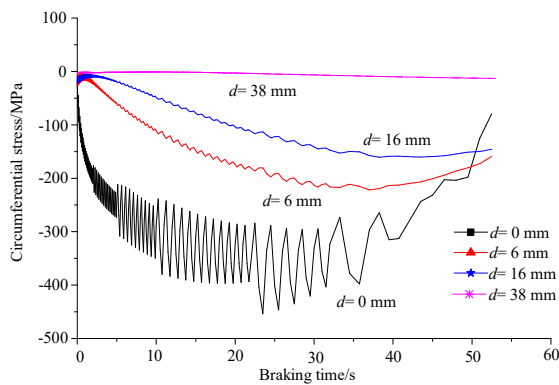
4.2. Stress field results

Using the indirect coupling method, the analysis result of the temperature field is applied as a load to the

simulation analysis of the thermal stress. The element type was also changed from SOLID70 to SOLID185, and full constraints were imposed on the bolt holes [49-50]. The nodes at $d=0$ mm, 6 mm, 16 mm, and 38 mm from the disc surface position are selected in turn, and the change curves of circumferential stress, radial stress and equivalent stress with braking time are studied respectively. Figures 9-12 are once 200 km/h emergency braking, once 300 km/h emergency braking, once 29 kN constant pressure braking, and three times of 29 kN successive constant pressure braking curves of thermal stress along the thickness and radial directions. The cloud diagram of brake disc transient stress field under different working conditions is shown in Figure 13.

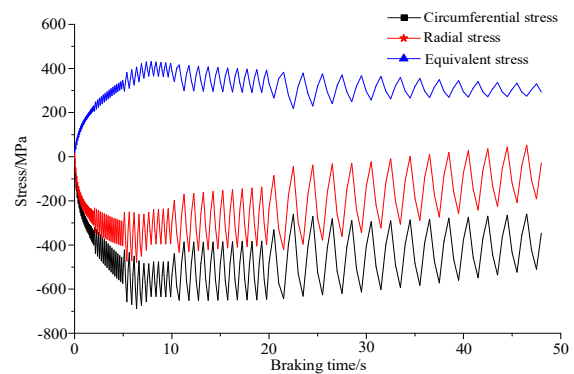


(a) Transient thermal stress change curve of the brake disk surface

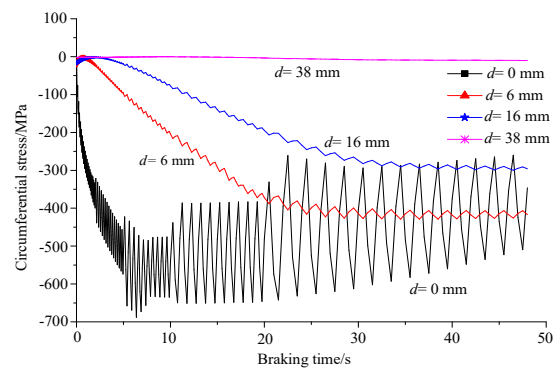


(b) Thermal stress variation curve of circumferential stress along the thickness direction

Figure 9. 200 km/h emergency braking

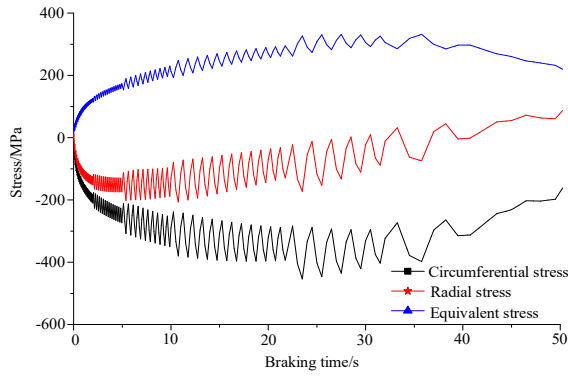


(a) Transient thermal stress change curve of the brake disk surface

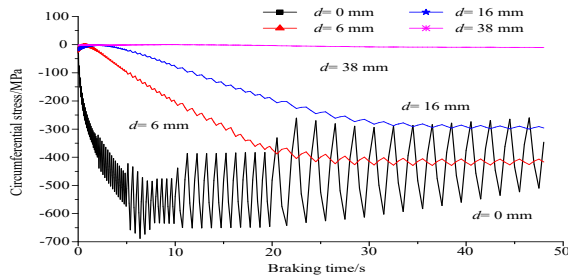


(b) Thermal stress variation curve of circumferential stress along the thickness direction

Figure 10. 300 km/h emergency braking

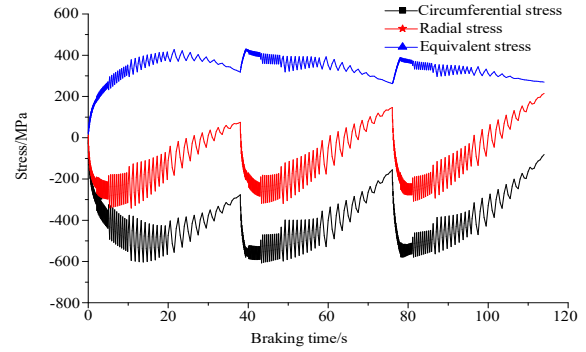


(a) Transient thermal stress change curve of the brake disk surface

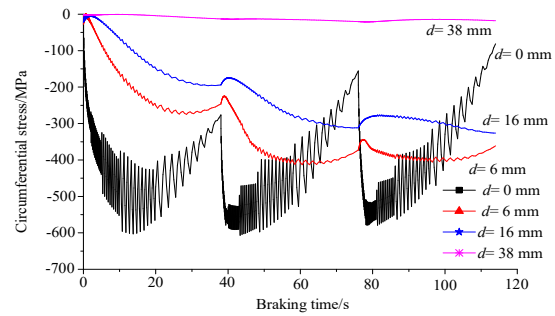


(b) Thermal stress variation curve of circumferential stress along the thickness direction

Figure 11. 29 kN constant pressure braking

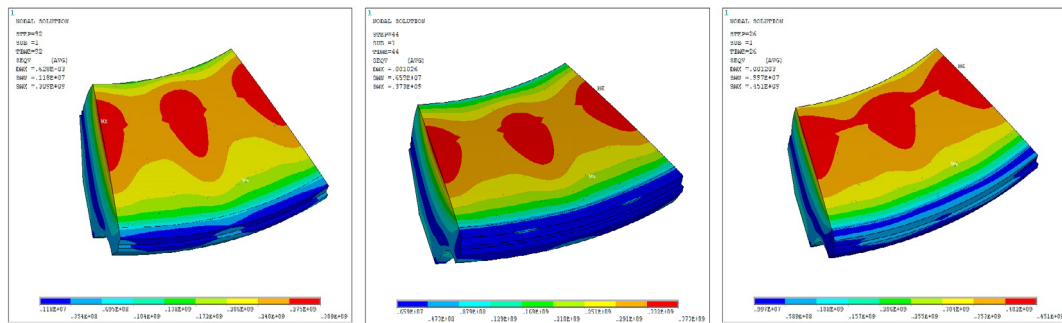


(a) Transient thermal stress change curve of the brake disk surface



(b) Thermal stress variation curve of circumferential stress along the thickness direction

Figure 12. Three times of 29 kN successive constant pressure braking



(a) 200 km/h emergency braking (b) 29 kN constant pressure braking (c) 300 km/h emergency braking

Figure 13. The stress field cloud diagram under different braking conditions

The main conclusions are as follows:

1. Under four different braking conditions, the circumferential stress of the disc surface is obviously greater than the radial stress.
2. During the braking process, the circumferential stress is dominant, which indicates that the surface is dominated by radial cracks; The rapid decline of the circumferential stress indicates that the radial cracks are mainly based on shallow cracks. When d is larger in the depth direction, the crack loses its driving force for growth. Radial cracks are one of the important reasons restricting train safety.
3. From the thermal stress curve of the brake disc, it can be seen that under four different working conditions, the stress is dominated by compressive stress during braking. After braking, a residual tensile stress of different magnitudes is formed under room temperature.

4. The change trend of the circumferential stress along the radial direction is similar to the change trend of the temperature field along the radial direction. The circumferential compressive stress reaches the maximum at about $l = 263$ mm (at the center of the friction ring); At $l = 223$ mm-263 mm and $l = 263$ mm-303 mm, the value gradually decreases; The circumferential stress values at $l = 243$ mm and $l = 283$ mm are not much different. It can be seen that the circumferential stress is almost symmetrical in the radial direction.
5. The thermal stress under 300 km/h emergency braking is greater than the thermal stress of three times of 29 kN successive constant pressure braking, once 29 kN constant pressure braking, and once 200 km/h emergency braking in turn.

It is found that there are three main reasons for the damage of the brake disc: (1) After the brake disc is heated

by friction, the temperature increases, resulting in the combined burning of the friction surface; (2) Abrasive wear caused by road dust and hard spots falling off the worn surface; (3) Fatigue damage caused by thermal stress caused by friction between brake disc and brake pad. To sum up, when the maximum temperature of the brake disc exceeds the maximum allowable temperature, or the maximum stress exceeds the yield stress, it will cause great damage to the brake disc. You can select better high-temperature and high-strength materials or optimize the heat dissipation structure of the brake disc, and add some grooves on the brake disc to reduce the temperature during the use of the brake disc, at the same time, the occurrence of severe working conditions such as emergency braking should be minimized, or the operating speed should be reduced to prolong the service life of the brake disc.

5. Conclusions

It can be inferred from simulation results that:

1. Although the braking conditions are different, the temperature change of the disk surface has similar laws from the temperature change curve. At the beginning of braking, with the continuous input of strong heat flow, the disk surface rises rapidly in a very short time and reaches the peak point soon. Then, due to the effect of forced convective cooling, the disk body gradually dissipates heat through radiation and convection, and the temperature decreases slowly.
2. The temperature of the brake disc surface is the highest. Along the depth direction, the farther away from the friction surface, the lower the temperature. The temperature in the center of the friction ring is the highest. Along the radius direction, the farther away from the center of the friction ring, the lower the temperature. The equivalent stress produced by the once 300 km/h emergency braking is the largest. It can be seen that speed has the greatest impact on the stress field of brake disc.
3. The three times of 29 kN successive constant pressure braking, the thermal stress in the second time is the largest and greater than the thermal stress formed during the first and third braking, while the temperature field is different. The maximum temperature in the latter time is greater than the previous. This is because the higher the temperature, the smaller the yield limit of the forged steel material, and the easier the material enters the plastic zone. The maximum equivalent stress produced by the third constant pressure braking is less than 10%, which shows that the damage caused by the third continuous braking is large.
4. According to the above research results, based on the bionic design concept, some new bionic heat dissipation ribs should be proposed to reduce the temperature field and stress field of the brake disc, so as to provide reference for the structural optimization and design of the brake disc.

Acknowledgments

The project supported by Scientific and Technological Innovation Programs of Higher Education Institutions in Shanxi (grant number: 2021L567); Luliang Development

Zone High-Level Science and Technology Talent Introduction Program (grant number: Rc2020-116).

Reference

- [1] Shi, X.L. Research on thermal fatigue life evaluation of high speed train on forging brake disc. PHD. Thesis, Beijing Jiaotong University, Beijing, 2016.
- [2] Zhao, K.K., Jiang, P.F., Feng, Y.J., et al. Investigation of the characteristics of hydraulic fracture initiation by using maximum tangential stress criterion. *Journal of Mining and Strata Control Engineering*, 2021, 3(2), 023520.
- [3] Jian, Q.F., Li, W., Yan, S. Thermal analysis of ventilated brake disc based on heat transfer enhancement of heat pipe. *International Journal of Thermal Sciences*, 2020, 155, 106356.
- [4] Mori, K.S., Peng, H.M. Causes and countermeasures of thermal fatigue of brake disc. *Foreign Rolling Stock Technology*, 2009, (3), 38-41.
- [5] Chen, G.B., Li, T., Yang, L., et al. Mechanical properties and failure mechanism of combined bodies with different coal-rock ratios and combinations. *Journal of Mining and Strata Control Engineering*, 2021, 3(2), 023522.
- [6] Stepan, A., Mikhailenko, M.A., Sheremet. Impacts of rotation and local element of variable heat generation on convective heat transfer in a partially porous cavity using local thermal non-equilibrium model. *International Journal of Thermal Sciences*, 2020, 155, 106427.
- [7] Wu, S.C, Zhang, S.Q, Xu, Z.W. Thermal crack growth-based fatigue life prediction due to braking for a high-speed railway brake disc. *International Journal of Fatigue*, 2016, 87, 359-369.
- [8] Yevtushenko, A.A., Kuciej, M., Grzes, P., et al. Temperature in the railway disc brake at a repetitive short-term mode of braking. *International Communications in Heat and Mass Transfer*, 2017, 84, 102-109.
- [9] Zhao, C., Wang, C.L., Wang, R.N., et al. Research on thermal performance simulation of ventilated brake disc based on ABAQUS. *Drive System Technique*, 2021, 35(3), 3-7.
- [10] Srivastava, A.K., Arora, P.K., Kumar, H., et al. Numerical and experiment fracture modeling for multiple cracks of a finite aluminum plate. *International Journal of Mechanical Sciences*, 2016, 110, 1-13.
- [11] Li, J., Li, L., Wu, J.P. Analysis of the temperature field during the sliding process of friction pair of brake disc. *Journal of Beijing Information Science & Technology University*, 2020, 35(6):43-49.
- [12] Yang, Y., Ye, X.L., Ye, C. Analysis and optimization of thermal performance of brake disc of ultra deep mine hoist. *Chinese Journal of Engineering Design*, 2019, 26(1), 47-55.
- [13] Collignon, M., Cristol, A.L., Dufrenoy, P., et al. Failure of truck brake disc: A coupled numerical-experimental approach to identifying critical thermomechanical loadings. *Tribology International*, 2013, 59(1), 114-120.
- [14] Yevtushenko, A.A., Greza, P. Mutual influence of the velocity and temperature in the axisymmetric FE model of a disc brake. *International Communications in Heat and Mass Transfer*, 2014, 57, 341-346.
- [15] Anderson, A.E., Knapp, R.A. Hot spotting in automotive friction systems. *Wear* 1990, 135(2), 319-337.
- [16] Belhocine, A., Bouchetara, M. Investigation of temperature and thermal stress in ventilated disc brake based on 3D thermomechanical coupling model. *Ain Shams Engineering Journal* 2013, 4(3), 475-483.
- [17] Ghadimi, B., Sajedi, R., Kowsary, F. 3D investigation of thermal stresses in a locomotive ventilated brake disc based on a conjugate thermo-fluid coupling boundary conditions.

- International Communications in Heat and Mass Transfer, 2013, (49), 104-109.
- [18] Choj, J.H., Lee, I. Finite element analysis of transient thermoelastic behaviors in disk brakes. *Wear* 2004, 257(1-2), 47-58.
- [19] Su, S.L., Du, Y., Zhu, J.F., et al. Numerical study on bearing behavior of layered rock mass for deep roadway. *Journal of Mining and Strata Control Engineering*, 2020, 2(1), 013002.
- [20] Gao, F., Wu, B.W., Yang, J.Y. Relationship of pad material parameters and brake disc temperature field. *The Chinese Journal of Nonferrous Metals*, 2020, 30(4), 837-846.
- [21] Kim, D.J., Lee, Y.M., Park, J.S., et al. Thermal stress analysis for a disk brake of railway vehicles with consideration of the pressure distribution on a frictional surface. *Materials Science and Engineering: A*, 2007, 483, 456-459.
- [22] Adamowicz, A., Grzes, P. Analysis of disc brake temperature distribution during single braking under non-axisymmetric load. *Applied Thermal Engineering*, 2011, 31(6-7), 1003-1012.
- [23] Li, Y.M., Yang, J.Y., Han, X.M., et al. Influence of contact area and contact mode on temperature field of brake disc. *Railway Locomotive & Car*, 2020, 40(3), 23-28.
- [24] Zhu, G., Huang, S.T., Xu, L.F., et al. Simulation and analysis of temperature field of SiCp/Al composite brake disc. *Ordnance Material Science and Engineering*, 2019, 42(6), 44-50.
- [25] Chai, J., Ouyang, Y.B., Zhang, D.D. Crack detection method in similar material models based on DIC. *Journal of Mining and Strata Control Engineering*, 2020, 2(2), 023015.
- [26] Chernyshov, E.A., Romanov, A.D., Romanov, I.D., et al. Evaluation of the Possibility of Replacement of an SCH24 Cast Iron of Detail of a "Brake Disc" of a Car by an Aluminum-Based Dispersion-Strengthened Composition Material Prepared by Internal Oxidation. *Journal of Machinery Manufacture and Reliability*, 2021, 50(1), 34-40.
- [27] Chen, J.W. Analysis of road header's rotary table on vibration modal based on finite element method and tested data. *Journal of Mining and Strata Control Engineering*, 2020, 2(2), 026032.
- [28] Chu, M.Z., Su, C., Mi, X.Z. Transient temperature field simulation analysis of high speed brake disc based on infinitesimal element method. *Manufacturing Automation*, 2020, 42(3), 79-84.
- [29] Wu, B., Sun, L. Study on transient temperature field of brake disc based on fluid-solid coupling heat transfer. *Machinery Design & Manufacture*, 2020, 6, 117-120.
- [30] Sha, Z.H., Li, C.X., Liu, Y., et al. Effect of groove surface features on temperature field and stress field of brake disc in braking process. *Machine Tool & Hydraulics*, 2020, 48(11), 128-133.
- [31] Zhang, B.L., Shen, B.T., Zhang, J.H., et al. Experimental study of edge-opened cracks propagation in rock-like materials. *Journal of Mining and Strata Control Engineering*, 2020, 2(3), 033035.
- [32] Cai, Y.F., Li, X.J., Deng, W.N., et al. Simulation of surface movement and deformation rules and detriment key parameters in high-strength mining. *Journal of Mining and Strata Control Engineering*, 2020, 2(4), 043511.
- [33] Ripley, M.I., Kirstein, O. Residual stresses in a cast iron automotive brake disc rotor. *Physica B Condensed Matter*, 2006, 385, 604-606.
- [34] Yousuf, L.S. The effect of temperature on the stresses analysis of composites laminate plate. *Jordan Journal of Mechanical and Industrial Engineering*, 2019, 13(4), 265-269.
- [35] Chiou, Y.J., Lee, Y.M., Tsay, R.J. Mixed mode fracture propagation by manifold method. *International Journal of Fracture*, 2002, 114(4), 327-347.
- [36] Kheder, A.R.I., Jubeh, N.M., Tahah, E.M. Fatigue properties under constant stress/variable stress amplitude and coaxing effect of acicular ductile iron and 42 CrMo4 steel. *Jordan Journal of Mechanical and Industrial Engineering*, 2011, 5(4), 301-306.
- [37] Teng, C.Q., Wang, L., Wei, P., et al. Parameter inversion of probability integral prediction based on shuffled frog leaping algorithm. *Journal of Mining and Strata Control Engineering*, 2020, 2(4), 047038.
- [38] Zhou, S.X., Guo, Z.H., Bai, X.Y. Fatigue fracture analysis of brake disc bolts under continuous braking condition. *Engineering Failure Analysis*, 2020, 115, 104588.
- [39] Khandakji, K.A. Analysis of hoisting electric drive systems in braking modes. *Jordan Journal of Mechanical and Industrial Engineering*, 2012, 6(2), 141-145.
- [40] Alshyyab, A.S., Darwish, F.H. Three-dimensional stress analysis around rivet holes in a plate subjected to biaxial loading. *Jordan Journal of Mechanical and Industrial Engineering*, 2018, 12(4), 323-330.
- [41] Tsay, R., Chiou, Y., Chuang, W. Crack growth prediction by manifold method. *Journal of Engineering Mechanics*, 1999, 128(8), 884-890.
- [42] Li, Z.Q., Han, J.M., Yang, Z.Y., et al. Analyzing the mechanisms of thermal fatigue and phase change of steel used in brake discs. *Engineering Failure Analysis*, 2015, (57), 202-218.
- [43] Wang, D.L., Hao, B.Y., Liang, X.M. Slurry diffusion of single fracture based on fluid-solid coupling. *Journal of Mining and Strata Control Engineering*, 2021, 3(1), 013038.
- [44] Parameswaran, V., Sharma, S. Estimation of fracture parameters and stress field for edge cracks in finite elastically graded plates using boundary collocation. *Acta Mechanica*, 2006, 184(4), 159-170.
- [45] Neimitz, A., Dzioba, I. The influence of the out-of- and in-plane constraint on fracture toughness of high strength steel in the ductile to brittle transition temperature range. *Engineering Fracture Mechanics*, 2015, 147, 431-448.
- [46] Chen, A., Kienhöfer, F. The failure prediction of a brake disc due to nonthermal or mechanical stresses. *Engineering failure analysis*, 2021, 124, 105319.
- [47] Yu, X.Y., Wang, Z.S., Yang, Y., et al. Movement rule of overburden in fully mechanized caving mining with thick depth and high mining height based on 3DEC. *Journal of Mining and Strata Control Engineering*, 2021, 3(1), 013533.
- [48] Wallis, L., Leonardi, E., Milton, B., et al. Air flow and heat transfer in ventilated disc brake rotors with diamond and tear-drop pillars. *Numerical Heat Transfer Applications, Part A*, 2002, 41(6-7), 643-655.
- [49] Duzgun, M. Investigation of thermo-structural behaviors of different ventilation applications on brake discs. *Journal of Mechanical Science and Technology*, 2012, 26(1), 235-240.
- [50] Mcclung, R.C., Sehitoglu, H. On the finite element analysis of fatigue crack closure-1. Basic modeling issues. *Edward Elgar*, 1989, 33(2), 237-252.